

# Normalised Equi-Angular Recognition Technique of Human Ear Signatures for Use in Biometrics Applications

Ghassan A. Al-Kindi, *Senior member, IACSIT* and Brian C. Lovell

**Abstract**—Human ear is perhaps one of the relatively promising features that can be used in biometrics applications. Hence, the aim of this work is to assess the validity of using human ear recognition in real biometrics applications. A proposed system for ear recognition is presented and experimentally tested. The system employs equiangular ear signatures. Cross Correlation Function (CCF) is employed in the system to find best angular match and apply angular shift to ear-signatures accordingly. Image scene size problem is overcome by using normalised values of the ear-signatures. Re-arrangements of the ear-signature data set is applied using equiangular steps where equally stepped size angles are used to acquire signature data set of same and fixed length array points, hence, comparison and matching of point to point can be readily applicable. Two parameters, namely error energy and Pareto's-based indicator, to assess the signature similarities are proposed and used in the investigation. Results showed the validity of the approach and encourage the adopting of the developed technique in real applications.

**Index Terms**—Ear biometrics, ear matching, human ear recognition.

## I. INTRODUCTION

The use of biometrics has become a core research area due to the growing demand and the need of reliable techniques that are readily applicable in real applications. One of the promising biometric features is the human ear. This is due to that [1]:

- Human ear has a dedicated shape for each individual.
- Human ears are less affected by aging and muscle tension/relaxation compared to human faces.

It has been stated that the importance of ear in establishing identity was realised by Imhofer in the year 1906 [2]. Today, possible application areas for the use of human ear as a biometric feature may include security, surveillance, and other civil oriented applications.

Detecting of ear shape from an image of arbitrary orientation of human face is a challenging problem due to that ear images can vary in appearance from different viewing angles and illumination conditions. Recognition and matching of detected ear shapes present additional challenging task. In spite of the already conducted research work, there is a need to develop techniques with better invariance, perhaps more model based, and to seek out high speed recognition techniques to cope with the very large datasets that are likely to be encountered in practice [3].

Investigation of human ear detection and recognition is gaining more research attention in recent years [4]. Different techniques for human ear detection and recognition were attempted by a number of researchers e.g. [5-15], however, the conducted literature review strongly assures that although a number of attempts were made more research investigations are required to develop reliable and more robust techniques in the areas of detection, feature extraction and recognition in order to facilitate the implementation of ear biometrics in real applications. In this work a system for ear recognition is proposed, experimentally tested and evaluated.

Fig. 1 presents the anatomy of the human ear. It should be noted that the ear does not have a completely random structure but it is made up of standard features [3].

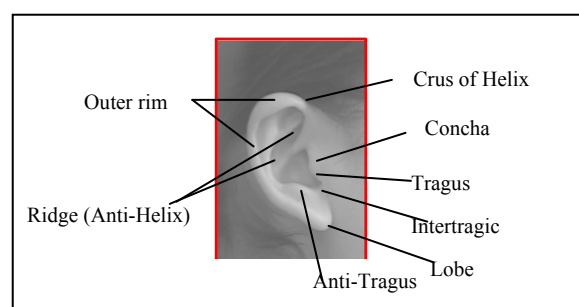


Fig. 1. Human ear anatomy..

## II. THE PROPOSED SYSTEM FOR HUMAN EAR RECOGNITION

The block diagram of the proposed and developed system is shown in Fig. 2. The system assumes that the ear is clearly visible to the vision system with adequate resolution. In addition the system uses a fixed camera position and aims to overcome the problems associated with image size as well as angular orientation due to "Pitch" angular movement. Handling of problems associated with "Yaw" and "Roll" angular movements are not included in the current study, however, planned for future work. The system aims to recognise and measure the similarity of ear image with a reference based on the outer rim and lobe as these two ear features form the outer profile of the ear shape.

The system starts by loading image data and acquire closed loop contour of the ear shape using a traditional method of feature extraction presented in [16]. Centroid of all boundary points is then calculated:

$$X_{Centroid} = \frac{1}{N} \sum_{n=1}^N x_n \text{ and } Y_{Centroid} = \frac{1}{N} \sum_{n=1}^N y_n$$

where  $N$  is the total number of points in the contour array,  $x_n$  and  $y_n$  are the coordinates of point  $n$  in the array, and  $(X_{Centroid}, Y_{Centroid})$  is the centroid coordinates.

Manuscript received April 4, 2012; revised May 1, 2012.

G. A. Al-Kindi is with Sohar University, Oman (e-mail: gkindi@soharuni.edu.om).

B. C. Lovell is with the University of Queensland, Brisbane, Australia (email: lovell@itee.uq.edu.au).

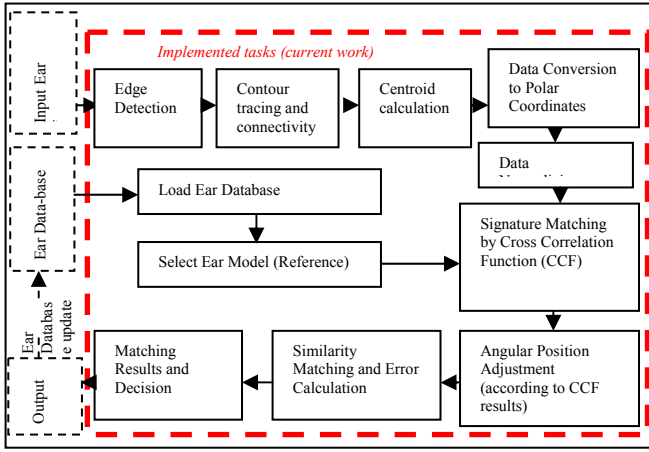


Fig. 2. Proposed human ear biometric system.

Knowing that the polar coordinates of object contours are the contour signatures, the next step in the process is to convert the contour point coordinates, (for both the reference and the image under investigation contours), into polar  $(r, \theta)$  presentation. This can be achieved by application of:

$$\theta_n = \tan^{-1} \left( \frac{y - Y_{Centroid}}{x - X_{Centroid}} \right) \quad (1)$$

$$r_n = \sqrt{(x - X_{Centroid})^2 + (y - Y_{Centroid})^2} \quad (2)$$

The outcome from this process concludes arrays having  $N$  points. However, the number of points  $N$  in each array differs according to the size of the ear, image resolution, digitization limitation, as well as other influences related to camera distance from the object. Hence because of the different array lengths, point to point array comparison cannot be applied.

To overcome such drawback, a re-calculation of the polar coordinates of contour points using unit steps of angle  $\theta$  is required to be carried out by interpolation, therefore equal length data from different size arrays are acquired; step angles can be selected to suit the image resolution and the required accuracy. In the current work the step size angle is set to  $1^\circ$  hence each contour signature length is 360 points.

The problem of image size is overcome by normalising the radii components of the contour polar coordinates:

$$r_{norm_n} = \frac{r_n}{r_{max}} \quad \text{for } n=1, 2, 3, \dots, N \quad (3)$$

where  $r_{max}$  is the maximum value of all radii components in the signature array of the contour.

Next step of the process is to eliminate the angular orientation problem. This is achieved by application of cross correlation and re-arranging signature data according to the maximum value of correlation outcome and its angle.

Having two sets of  $N$  elements signature radii arrays namely the reference  $R_1(n)$  and the signature under investigation  $R_2(n)$ , the cross correlation function CCF can be defined as:

$$CCF(k) = \sum_{n=1}^N R_1(n) \times R_2(n+k) \quad (4)$$

where  $k$  is the shift value and has the values  $k=1,2,3,\dots,N$ .

The maximum value of  $CCF(k)$  presents the best match between the two sets of signature radii data which occur at  $k$  elements shift of the  $R_2$  set of data.

One advantage gained from the closed loop contours of the

ear is its periodicity over each complete cycle, hence:

$$R_1(N+k) = R_1(k) \text{ and } R_2(N+k) = R_2(k)$$

where  $k=1,2,3,\dots,N$ .

Therefore the computation of the CCF will imply equal set of iterative multiplication for  $k=1$  to  $k=N$ .

Based on the outcome from the application of the CCF, the data set  $R_2$  can now be re-arranged as follow:

$$\bar{R}_2(n) = R_2(N+n-\bar{k}) \text{ for } n=1,2,3,\dots,N \quad (5)$$

where  $\bar{k}$  is the angular shift value that produce maximum value of CCF.

Once this stage is completed the two signature radii data sets become ready to be implemented in point by point comparison. Hence a deviation error, signature comparison error, to record the output of the comparison process can be defined as:

$$E(n) = |R_1(n) - R_2(n)| \text{ for } n=1,2,3,\dots,N \quad (6)$$

The output  $E(n)$  from the comparison process can be then statistically analysed with proper selection of threshold value levels to decide whether the two compared sets are positively matched or unmatched. One parameter that could be used to measure the similarity of compared signature pairs is the "error energy" parameter which is defined as the area under the acquired error curve. In other words the error energy parameter  $E_{energy}$  is:

$$E_{energy} = \sum_{n=1}^N E(n) \quad (7)$$

Never the less, Pareto's "vital few and trivial many" 80/20 rule may also be applied to calculate the error energy of the largest 20% of the resulting  $E(n)$  computed according to Equation 6. This can be carried out by re-arranging the elements of  $E(n)$  from largest to smallest and summing the error values associated with the first 20% of the elements; the 20% of the conducted experiment in this article is 72 elements.

In reality, the successfulness of these measures depends on whether a distinguished threshold value can be identified for each to properly classify matched and unmatched pairs of ear profile signatures.

### III. RESULTS AND DISCUSSIONS

A large number of experiments were conducted using different sets of images to assess the developed methodology. Fig. 3 presents examples of some images used in the investigation. Images S1 to S9 presented in the Figure are extracted from the USTB database [17], whereas images S10 to S18 in the same Figure are samples from a set of human ear images acquired by the authors of this article. These images show human ears of different persons which are acquired from various orientations and scene sizes having an average image resolution of 400x400 pixels.

The proposed system is implemented to acquire the closed loop contour of the outside ear shape together with the generation of the boundary polar coordinates, (profile signature), and boundary centroid. An angular step size of  $1^\circ$  is used to acquire the radii set of the profile signature, hence each signature include a set of 360 radii values.

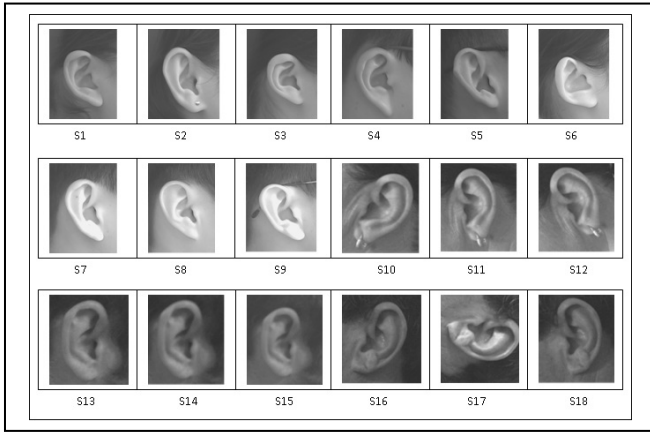


Fig. 3. Human ear image examples.

Fig. 4 provides examples of the resulting profile signatures for the image samples given in Fig. 3. It could be observed from this Figure that signature profile of images (S1, S2, and S3), (S7, S8, and S9), and (S13, S14, and S15) sets have considerably similar angular arrangements of their patterns that minimum angular shift could be noticed. However signature profile of (S4, S5, and S6), (S10, S11, and S12), and (S16, S17, and S18) sets of images clearly demonstrate larger angular shift arrangement of their patterns. This is due to the angular orientation of the ear within each image sample, hence application of cross correlation to find best angular match of the signature profile would help to enable the re-arrangements of the signature radii sets to establish best match between each signature profile pairs.

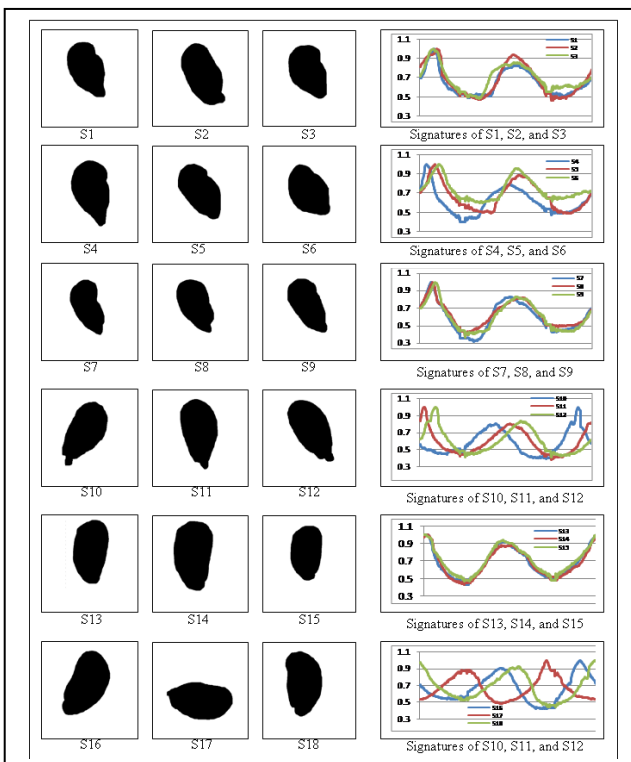


Fig. 4. Examples of acquired ear profile signatures.

Examples of CCF results are given in Fig. 5.a and 5.f for the image pairs S9andS14 and S14andS15 respectively. The resulting best angular correlation between S9andS14 is found to be at  $359^\circ$  ( $-1^\circ$ ) whereas it is found to be at  $27^\circ$  ( $-333^\circ$ ) for the signature pair S14andS15. Sample results of angular shift process of the signature profiles to match best correlation are

given in Figs. 5.b and Fig. 5.g for the same pairs respectively. Reconstructions of the ear profiles at their best correlated positions are represented in Fig. 5.c and 5.h respectively. Acquired error values  $E(n)$  using Equation 6 for the two comparisons are plotted in Fig. 5.d and Fig. 5.i where the total error energy, (i.e. the area under the curve), is (21.979) in case of comparing S9andS14 which is larger in value than S14andS15 signature comparison due to the differences in the compared profile signatures. In the case of S14andS15 comparison, the computed error energy value is (9.445). However to reach a concrete decision of whether the two signature pairs are of the same ear a valid threshold value of the computed error energy to classify signature pairs must exist and be found.

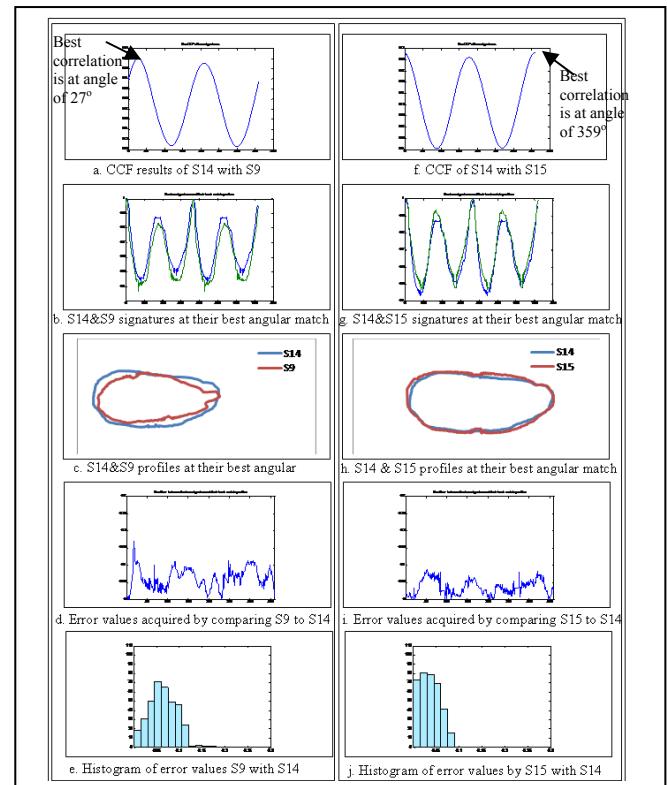


Fig. 5. Example results of ear matching.

Hence a number of tests were conducted to verify the existence of such threshold value. Table I lists examples of acquired results from several conducted comparisons. A threshold value of 11 is found to be valid for the error energy parameter; therefore, this value is used in the decision making. However, it can be observed that although a valid decision is gained from the proposed procedure due to the proper selection of the error energy threshold value, the acquired error energies, in some comparison cases, are close to the selected threshold value from both sides. This dictates that the use of error energy parameter alone in the decision process is a critical issue and may lead, in some cases, to false identification/classification of human ears. In order to enhance the reliability of the results, another key indicator is introduced which is based on histogram analysis of resulting error values. Fig. 5.e and 5.j show constructed histograms of two conducted comparisons, namely S9andS14 and S14andS15 respectively. The error values in each array are distributed into a number of bins. A range of 0.015 is selected for each bin in the conducted trials. It is obvious from these

figures that the resulting histograms while comparing different pairs of ear signatures take wider distribution hence bin heights in this case are of small heights, whereas in the case of comparing similar ear profiles the number of histogram bins are less in number and these bins are characterised by more height which indicate less value of error resulting from the comparison process. However reliable numerical measures or threshold values cannot be always identified. Hence, an alternative indicator based on

Pareto's principle is investigated. The sum of error values resulting from the highest 20% of elements in each error array is calculated and included in Table I. It is evident from these results that based on Pareto's principle a valid threshold value could be found; in the conducted tests the threshold value based on Pareto's principle is found to be 4.5. However, to ensure a definite separation between match/un-match cases both the error energy parameter and Pareto's-based indicator can be used together to provide precise matching decision.

TABLE I: EXAMPLE OF ACQUIRED EAR RECOGNITION RESULTS

Ear Signatures Compared	Comments on the Compared Signatures	Best Match Angle	Error Energy $E_{energy}$	Pareto's 20% sum of errors	Decision based on Acquired Results
S2 with S2R	Same ear with one of which rotated by 90o	90o	3.142	1.711	Positively matched
S10 with S11	Same ear one of which is rotated.	38o	5.245	2.675	Positively matched
S14 with S13	Same ear one of which with smaller view size and slightly rotated.	356o	5.702	2.597	Positively matched
S11 with S12	Same ear one of which with smaller view size and rotated.	22o	6.475	2.954	Positively matched
S17 with S18	Same ear one of which with smaller view size and rotated.	99o	8.511	3.588	Positively matched
S16 with S18	Same ear one of which with smaller view size and rotated.	29o	8.733	3.965	Positively matched
S10 with S12	Same ear one of which with smaller size view and rotated.	61o	8.765	4.103	Positively matched
S16 with S17	Same ear one of which with smaller view size and rotated.	290o	9.016	5.329	Positively matched
S14 with S15	Same ear one of which with smaller view size and slightly rotated.	359o	9.445	4.936	Positively matched
S13 with S15	Same ear one of which with smaller view size and slightly rotated.	2o	10.252	3.998	Positively matched
S14 with S2	Different ears though having close ear contours and one of them is rotated	25o	11.397	5.104	Different ears
S14 with S3	Different ear signatures and one of them is rotated	24o	13.409	6.149	Different ears
S14 with S5	Different ear signatures and one of them is rotated	33o	13.573	6.179	Different ears
S4 with S7	Different ear signatures	8o	13.634	6.211	Different ears
S14 with S18	Different ears, one is right hand side whereas the other is left hand side and rotated	188o	14.499	6.437	Different ears
S14 with S17	Different ears, one is right hand side whereas the other is left hand side and rotated	88o	14.975	6.499	Different ears
S14 with S1	Different ear signatures and one of them is rotated	24o	15.178	7.035	Different ears
S14 with S8	Different ear signatures and one of them is rotated	24o	15.284	7.057	Different ears
S14 with S16	Different ears, one is right hand side whereas the other is left hand side and rotated	159o	16.962	7.149	Different ears
S1 with S3	Different ear signatures	0o	18.612	8.742	Different ears
S14 with S9	Different ear signatures and one of them is rotated	27o	21.979	7.593	Different ears
S14 with S4	Different ear signatures and one of them is rotated	13o	22.286	9.471	Different ears
S14 with S6	Different ear signatures and one of them is rotated	35o	25.133	11.118	Different ears
S14 with S7	Different ear signatures and one of them is rotated	21o	25.731	8.818	Different ears
S14 with S12	Different ear signatures, one is right hand side and the other is a rotated left hand side	28o	26.120	10.237	Different ears
S14 with S11	Different ears, one is right hand side whereas the other is left hand side and rotated	5o	28.336	11.122	Different ears
S14 with S10	Different ears, one is right hand side whereas the other is left hand side and rotated	328o	31.860	12.608	Different ears
S6 with S9	Considerably different ear signatures	353o	43.183	15.717	Different ears

To demonstrate the validity of the system to deal with rotated versions of the same ear profile Fig. 6.a show acquired signatures of the same ear pair though rotated by 90°. Fig. 6.b and 6.c give the resulting CCF and resulting signatures shifted to their best matching position. Result error values are plotted in Fig. 6.d whereas Fig. 6.e gives the resulting histogram of error values. It is evident from these results that this pair of signatures are positively matched due to that the resulting error energy value is 3.142 and Pareto's-based indicator is

1.711 where in both cases the errors are less than the identified threshold values.

Similar results were gained by comparing same ear though with different scene size, Fig. 6.f to 6.j. The proposed system has successfully distinguished the two signature pairs as of the same ear. In this case the resulting error energy is 8.733 and the resulting Pareto's-based indicator is 3.965. In both cases are less than the identified threshold values.

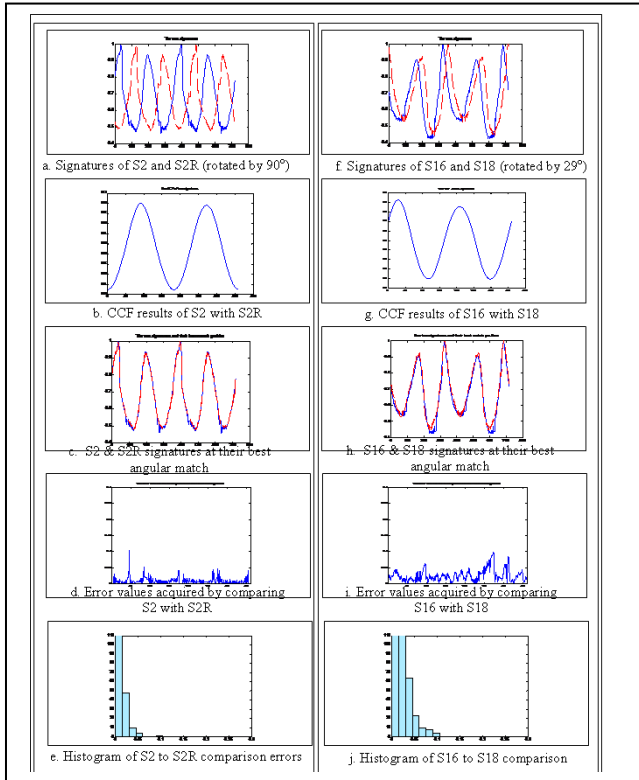


Fig. 6. Example results of ear signature matching.

#### IV. CONCLUSIONS

In this work a system is proposed and developed to recognise human ears. Its potential is evaluated through large number of conducted experiments using different types of human ear image data. It is evident from the acquired results that the proposed system is a valid technique to recognise and classify, with confidence, human ears according to their external shape attributes that include ears' outer rim and lobe. The system has showed to successfully overcome several problems associated with shape matching. In particular, polar coordinate-based signature has beneficially overcome the problems associated with shape orientations, the use of normalised radii has led to overcome the problems associated with image size and camera distance, and most importantly, the suggested use of equiangular radii data approach to re-generate the boundary signature has overcome the problems associated with varying length of boundary points in the image data of each signature, hence advantageously enabled the application of point by point data matching of signature pairs.

Results associated with ear shape matching using the proposed error energy parameter alone showed to yield several critical cases where false identification may result if the two compared signatures have a relatively similar shape profiles, hence the use of an additional error key indicator based on Pareto's analysis has successfully overcome the limitations associated with the use of error energy parameter alone.

#### REFERENCES

[1] A. Sana, P. Gupta, and R. Purkait, "Ear Biometrics: A New Approach," *International Conference on Advances in Pattern Recognition (ICAPR)*, Kolkata, India, 2007.

[2] R. Purkait, "Ear Biometric: An Aid to Personal Identification," *Anthropologist Special volume no. 3*, pp.215-218, 2007.

[3] D. J. Hurlley, B. Arbab-Zavar, and M. S. Nixon, "The Ear as a Biometric," *15th European Signal Processing Conference (EUSIPCO 2007)*, Poznan, Poland, September 3-7, pp. 25-29, 2007.

[4] D. Frejlichowski and N.Tyzkiewicz, "The West Pomeranian University of Technology Ear Database – A Tool for Testing Biometric Algorithms," A. Campilho and M. Kamel (Eds.): *ICIAR 2010, Part II, Lecture Notes in Computer Science*, vol. 6112, pp. 227–234, 2010.

[5] M. Ali, M. Y. Javed, and A. Basit, "Ear Recognition Using Wavelets," *Proceedings of Image and Vision Computing New Zealand*, pp. 83–86, 2007.

[6] F. Saleh, A. Hamdy, and F. Zaki, "Hybrid Features of Spatial Domain and Frequency Domain for Person Identification through Ear Biometrics," *Pattern Recognition and Image Analysis*, vol. 19, no. 1, pp. 35–38, 2009.

[7] S. Ansari and P. Gupta, "Localization of Ear Using Outer Helix Curve of the Ear," *IEEE Computer Society, Proceedings of the International Conference on Computing: Theory and Applications (ICCTA'07)*, 0-7695-2770-1/07, 2007.

[8] L. Nanni and A. Lumini, "A multi-matcher for ear authentication," *Pattern Recognition Letters* vol. 28, 2007, pp. 2219–2226.

[9] A. P. Yazdanpanah and K. Faez, "Normalizing Human Ear in Proportion to Size and Rotation," D. S. Huang et al. (Eds.): *ICIC 2009, LNCS 5754*, pp. 37–45, Springer-Verlag Berlin Heidelberg, 2009.

[10] M. Choraś, "Ear Biometrics Based on Geometrical Feature Extraction," *Electronic Letters on Computer Vision and Image Analysis* vol. 5, no. 3, pp. 84-95, 2005.

[11] S. Attarchi, Ka. Faez, and A. Raffei, "A New Segmentation Approach for Ear Recognition," J. Blanc-Talon et al. (Eds.): *ACIVS 2008, LNCS 5259*, pp. 1030–1037, Springer-Verlag Berlin Heidelberg, 2008.

[12] K. Chang, K. W. Bowyer, S. Sarkar, and Barnabas Victor, "Comparison and Combination of Ear and Face Images in Appearance-Based Biometrics," *IEEE Transactions on Pattern Analysis and Machine Intelligence*, vol. 25, no. 9, pp.1160-1165, September 2003.

[13] P. Yan and K. W. Bowyer, "Biometric Recognition Using 3D Ear Shape," *IEEE Transactions on Pattern Analysis and Machine Intelligence*, vol. 29, no. 8, pp. 1297-1308, August 2007.

[14] S. Cadavid and M. Abdel-Mottaleb, "3-D Ear Modeling and Recognition from Video Sequences using Shape from Shading," *IEEE Transactions on Information Forensics and Security*, vol. 3, no. 4, pp.709-718, December 2008.

[15] H. Chen and B. Bhanu, "Human Ear Recognition in 3D," *IEEE Transactions on Pattern Analysis and Machine Intelligence*, vol. 29, no. 4, pp. 718-737, April 2007.

[16] G. Al-Kindi, R. Baul, and K. Gill, "An Example of Automatic Two - Dimensional Component Inspection Using Computer Vision," *Proc Instn Mech Engrs, Part. B. Journal of Engineering Manufacture*, vol. 205, pp.71-83, 1991.

[17] Ear Recognition Lab. at the University of Science and Technology Beijing (USTB) <http://www1.ustb.edu.cn/resb/en/index.htm>.



**Ghassan A. Al-Kindi** was born in Baghdad, Iraq in 1963. He received the BSc in mechanical engineering in 1985 from the University of Technology (UOT), Iraq and received the PhD in mechanical engineering in 1990 from the University of Leeds, UK. He started his long time experience on image processing and pattern recognition in the 1986. Since then he published numerous number of research articles and supervised more than 40 PhD and MSc theses. One of his published articles won the 1989 Joseph Whitworth prize from the Institution of Mechanical Engineers IMechE, UK. He has also been honored with several national medals in recognition of his high distinct research outcome. Dr Al-Kindi is currently working as an Associate Professor at Sohar University, Oman. He is also an adjunct fellow to Queensland University, Australia. For the period 2005-2008 he became an honorary research associate to Monash University, Australia. He is currently an editorial board member of the International Journal of Image Processing IJIP and Journal on Image and Video Processing IJIVP. Dr Al-Kindi is a senior member of the IACSIT (International Association of Computer Science and Information Technology). He is also a member of several other engineering bodies and associations. During his last 26 years of research and industrial work, he has successfully handled and conducted many funded projects. The most recent of these is in the area of the development of vision system for

CNC machines to overcome their blindness; a project that is funded by Qatar National Research Fund QNRF.



**Brian C. Lovell** was born in Brisbane, Australia in 1960. He received the BEng in electrical engineering in 1982, the BSc in computer science in 1983, and the PhD in signal processing in 1991: all from the University of Queensland (UQ). Professor Lovell is Research Leader in National ICT Australia and Research Director of the Security and Surveillance Research group in the School of ITEE, UQ. He was President of the Australian Pattern

Recognition Society 1995-2005, Senior Member of the IEEE, Fellow of the World Innovation Forum, Fellow of the IEAust, and voting member for Australia on the governing board of the International Association for Pattern Recognition since 1998. Professor Lovell was Technical Co-chair of ICPR2006 in Hong Kong (Computer Vision and Image Analysis), and Program Co-chair of ICPR2008 in Tampa, Florida. He serves on the Editorial Board of Pattern Recognition Letters and reviews for many of the major journals in the fields of Computer Vision and Pattern Recognition. In March 2005, he was awarded Number 1 author at UQ with almost 35,000 copies of his papers downloaded from the UQ library archive. His research interests are currently focused on intelligent surveillance techniques, optimal image segmentation, real-time video analysis, and face recognition.